
Regression Trees Know Calculus

Nathan Wycoff

The McCourt School’s Massive Data Institute
 Georgetown University
 Washington, DC 20007
 nathan.wycoff@georgetown.edu

Abstract

Regression trees have emerged as a preeminent tool for solving real-world regression problems due to their ability to deal with nonlinearities, interaction effects and sharp discontinuities. In this article, we rather study regression trees applied to well-behaved, differentiable functions, and determine the relationship between node parameters and the local gradient of the function being approximated. We find a simple estimate of the gradient which can be efficiently computed using quantities exposed by popular tree learning libraries. This allows the tools developed in the context of differentiable algorithms, like neural nets and Gaussian processes, to be deployed to tree-based models. To demonstrate this, we study measures of model sensitivity defined in terms of integrals of gradients and demonstrate how to compute them for regression trees using the proposed gradient estimates. Quantitative and qualitative numerical experiments reveal the capability of gradients estimated by regression trees to improve predictive analysis, solve tasks in uncertainty quantification, and provide interpretation of model behavior.

1 Introduction

Tree-based methods, such as regression trees, are a workhorse of the contemporary data scientist. Their ease of use, computational efficiency and predictive capability without the need for extensive feature engineering makes them popular with practitioners. The most widely used version of regression trees approximate with greedily constructed, piecewise-constant functions than can handle data which exhibit discontinuities or divergent behavior in various parts of the feature-space. Perhaps because of their capability to tackle pathological problems, it seems that some of their properties in approximating well-behaved functions may have gone unnoticed.

In this article, we will study the approximation of a continuously differentiable function f on the unit cube in dimension P with a piecewise constant regression tree. In particular, we will investigate a means of approximating ∇f using only information contained in the tree structure in a single pass through the tree. We find a simple and easily computable quantity analogous to a finite difference which converges to the gradient of f in the large sample and infinite depth limit. Previously, gradient estimation in regression trees has been studied in the context where the leaves have differentiable models, and the gradients of these models are used to estimate the gradient (e.g. Chaudhuri et al. (1995); Loh (2011)). However, the constant-leaf tree remains prevalent in practice, and the purpose of this article is rather to examine the *implicit* gradient estimation that occurs within these constant-leaf trees where, formally, the gradient of the tree is almost-everywhere zero.

With a gradient estimator in hand, we unlock for tree-based models the stable of existing gradient-based methods for variable interpretation and dimension reduction developed in other areas. Among many possibilities, we will study in particular the Active Subspace Method (Constantine, 2015), a global dimension reduction technique from the Uncertainty Quantification literature, and the

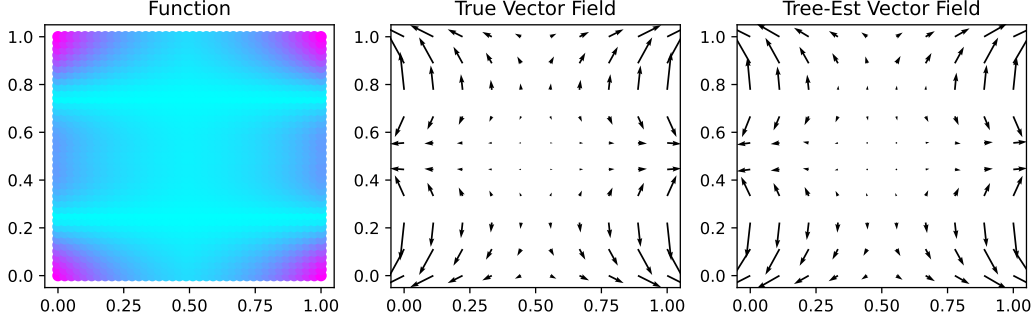


Figure 1: **Illustration of Gradient Estimates.** *Left:* Toy algebraic function. *Middle:* True vector field. *Right:* Tree-based vector field estimate using Algorithm 1.

Integrated Gradient Method (Sundararajan et al., 2017), a local model interpretation technique from the neural network literature.

Active Subspaces provide for linear dimension reduction, which is already commonly used in the setting of regression trees such as when using e.g. random projectin or PCA for rotated trees (Breiman, 2001; Rodriguez et al., 2006). In contrast to these methods, active subspaces consists of supervised linear dimension reduction which takes the relationship between features and response into account. Already, supervised linear dimension reduction has been proposed for use with tree based methods where, e.g. a kernel method is used to perform the dimension reduction which is then applied to a tree-based method (Shan et al., 2015). But here, we show how to actually use the tree itself to perform a linear sensitivity analysis, rather than relying on a helper model to do this. This is essential if the analyst is interested in *model*-interpretation (as contrasted with *data*-interpretation (Chen et al., 2020)), and to the best of our knowledge the application of the Active Subspace method, enabled by our novel gradient estimates, is the first such linear sensitivity metric for trees. And while we've so far discussed what active subspaces can do for regression trees, we don't think this new relationship will be one-sided. Our numerical experiments show that regression trees can serve as scalable estimators of the active subspace, favorable to existing methods along certain dimensions. We hope this can highlight the potential for regression trees in the UQ space.

We view the major contributions of our article as follows:

1. We develop a simple algorithm to extract gradient information from regression trees.
2. We show how to use this to port gradient-based interpretability techniques from other fields to benefit interpretability of regression trees.
3. We find that in certain circumstances gradient-enabled regression trees can produce better estimates of active subspaces than existing UQ methods.

We begin in Section 2 by discussing pertinent background on regression trees and gradient-based interpretability. Our main methodological contributions are given in Section 3 and 4 where we develop our gradient estimate. Subsequently, we illustrate these procedure on numerical examples in Section 5 before offering conclusions and future research directions in Section 6.

2 Background

While small decision trees are easily interpretable, they become significantly less so as they grow in size or if they are aggregated via Random Forests (Breiman, 2001, 2002) or gradient boosting (Friedman, 2001). Consequently, developing methods for increasing the interpretability of trees is of great importance (Louppe, 2014).

2.1 Variable Interpretation and Selection in Regression Trees

Several methods for variable importance were suggested alongside some of the original tree-based methods (Breiman, 2017, 2001, 2002), the two most salient for our study being the Mean Decrease in

Impurity (called MDI or TreeWeight Kazemitabar et al. (2017)) and the Feature Permutation method. MDI assigns importance to variables in proportion to the mean reduction in cost when splitting along a given variable, an intuitively reasonable approach. However, MDI as originally proposed was sensitive to properties of the feature variables as well as to the depth within the tree that a split occurred, leading to “debiased” variants (Sandri and Zuccolotto, 2008; Li et al., 2019). (Kazemitabar et al., 2017; Klusowski and Tian, 2020) studied theoretical properties of a simplified version of this metric using only the first split (“stumps”). On the other hand Feature Permutation is based on measuring decrease in performance when shuffling a given feature, and though the method does have some desirable properties (Ishwaran, 2007), it has come under criticism for undesirable behavior in the context of correlated predictors (Hooker et al., 2021). Empirical studies have found issues in both of these methods (Strobl et al., 2007, 2008). Against this backdrop of negative results on the behavior of these initially suggested methods came contributions in general-purpose machine learning interpretability methods. SHAP values (Lundberg and Lee, 2017) have been proposed as a general-purpose tool for understanding machine learning models. However, they would prove especially popular for understanding tree-based methods where efficient algorithms have been proposed for estimating these otherwise combinatorially difficult quantities (Lundberg et al., 2019; Karczmarz et al., 2022).

2.2 Gradient-based Model Interpretation

The gradient of a function tells us how its output is related to its input over short distances, and is a natural candidate to help explain the behavior of a model. Hechtlinger (2016) suggested to simply look at the gradient of a model evaluated at a particular observation to gain local understanding. Another approach is the Integrated Gradient (Sundararajan et al., 2017) introduced in the context of neural networks, which involves privileging some setting of input features which is called the *reference point*, which we’ll denote \mathbf{x}^* . Subsequently, in order to explain a prediction at a given point \mathbf{x} , we integrate the gradient along the path from \mathbf{x}^* to \mathbf{x} and multiply elementwise against that difference; that is, denoting the output of the neural network as f :

$$IG(\mathbf{x}) := (\mathbf{x} - \mathbf{x}^*) \odot \int_{\alpha=0}^1 \nabla f(\alpha \mathbf{x} + (1 - \alpha) \mathbf{x}^*) d\alpha. \quad (1)$$

This theoretically appealing approach has also seen practical success in applications including medicine (Sayres et al., 2019) and chemistry (McCloskey et al., 2019).

One could also integrate the gradient over a larger part of the space to perform a more global sensitivity analysis. This is the idea behind the Active Subspace Method Constantine (2015). In our context, this involves defining the Active Subspace Matrix as:

$$\mathbf{C}_\mu^f := \int_{[0,1]^P} \nabla f(\mathbf{x}) \nabla f(\mathbf{x})^\top d\mu(\mathbf{x}), \quad (2)$$

where μ is a measure. Eigenanalysis on \mathbf{C}_μ^f reveals linear combinations of features which are important, similar to PCA. Various techniques have been developed to estimate active subspaces in the presence only of input-output data. A Polynomial Ridge Approximation (PRA) procedure (Hokanson and Constantine, 2018) is available, as is a closed form estimate using Gaussian processes (GP) (Wycoff et al., 2021), and also an approach based on neural networks called the Deep Active Subspace Method (Tripathy and Bilionis, 2019; Edeling, 2023, DASM) has been proposed.

3 Behavior of Regression Trees Approximating Linear Functions

This section will study the properties of approximating a linear function on the unit hypercube $[0, 1]^P$ with a regression tree. We will first develop some notation. We will be concerned in this article with a sequence of nested dyadic trees of increasing depth. Each node in the tree will be associated with an integer i . $\mathcal{N}_i \subseteq \mathcal{X}$ is the set of points which map through the i th node on their way down the tree. C_i^l, C_i^r represents the left and right child of node i , respectively. Let $\mathcal{D}_k \subset \mathbb{N}^+$ denote all nodes which have depth k . $\mathbf{l}_i, \mathbf{u}_i \in [0, 1]^P$ denote the lower and upper bounds of the node i such that $\prod_{p=1}^P [l_{i,p}, u_{i,p}] = \mathcal{N}_i$. Each node is associated with a value $v_i \in \mathbb{R}$, which is the mean of the observations falling within it, and non-leaf nodes are split along some variable $\sigma_i \in \{1, \dots, P\}$ at

a threshold $\tau_i \in [l_{i,\sigma_i}, u_{i,\sigma_i}]$. At any depth k , the regions corresponding to \mathcal{D}^k form a partition of $[0, 1]^P$, and we denote by $B^k(\mathbf{x}) \in \mathbb{N}^+$ the index of the node of depth k containing \mathbf{x} .

The greedy tree splitting algorithm with MSE cost will construct the tree as follows. Say we have built a tree up to depth k . To build the next layer of depth $k + 1$, we must decide what the split variables σ_i and threshold values τ_i will be for each $i \in \mathcal{D}_k$. Denote by $C_i^l(t, s)$ the left child node that would be formed by cutting the i th node along variable s at t and define $C_i^r(t, s)$ similarly for the prospective right child node¹. To build the next level of depth we must decide on s and t , at which point they will become σ_i and τ_i . This is done by setting them to the values which minimize variance in each of the child nodes. In the large sample limit, this becomes equivalent to solving the following problem for all $i \in \mathcal{D}_k$:

$$\sigma_i, \tau_i = \operatorname{argmin}_{s \in \{1, \dots, P\}, t \in [l_{i,s}, u_{i,s}]} \mathbb{V}[f(\mathbf{x}); C_i^l(t, s)] + \mathbb{V}[f(\mathbf{x}); C_i^r(t, s)], \quad (3)$$

where

$$\mathbb{V}[f(\mathbf{x}); \mathcal{A}] := \frac{1}{|\mathcal{A}|} \int_{\mathcal{A}} \left(f(\mathbf{x}) - \mathbb{E}[f(\mathbf{x}), \mathcal{A}] \right)^2 d\mathbf{x}; \quad \mathbb{E}[f(\mathbf{x}), \mathcal{A}] := \frac{1}{|\mathcal{A}|} \int_{\mathcal{A}} f(\mathbf{x}) d\mathbf{x} \quad (4)$$

give the moments of the random variable $f(\mathbf{x})$ where \mathbf{x} is drawn uniformly at random from \mathcal{A} , and $|\mathcal{A}|$ gives the volume of the set \mathcal{A} .

3.1 Thresholding Behavior and Iteration

We are now prepared to study the large sample iteration behavior on linear functions $f(\mathbf{x}) = \mathbf{a}^\top \mathbf{x} + b$. As the sample size diverges, we have that $\mathbb{V}[\mathbf{a}^\top \mathbf{x}; [\mathbf{l}, \mathbf{u}]] = \frac{\sum_p a_p^2 (u_{i,p} - l_{i,p})^2}{12}$ such that that optimization may be rewritten as:

$$\operatorname{argmin}_{s \in \{1, \dots, P\}, t \in [l_{i,p}, u_{i,p}], p \neq s} 2 \sum_{p \neq s} a_p^2 (u_{i,p} - l_{i,p})^2 + a_s^2 \left((u_{i,s} - t)^2 + (t - l_{i,s})^2 \right). \quad (5)$$

For any fixed s , the minimum with respect to t occurs at $\frac{u_{i,s} + l_{i,s}}{2}$, yielding the profile problem:

$$\operatorname{argmin}_{s \in \{1, \dots, P\}} 2 \sum_{p \neq s} a_p^2 (u_{i,p} - l_{i,p})^2 + \frac{a_s^2}{2} (u_{i,s} - l_{i,s})^2. \quad (6)$$

By comparing any two costs, we can see that the s that will be chosen is that such that the quantity $|a_s|(u_{i,s} - l_{i,s})$ is maximized.

Such is the behavior for a specific node at a specific depth. Let's now reflect on what this implies for the iteration. Initially, $u_p - l_p = 1$ for all p , such that the variable with the largest coefficient p will be chosen for the first split; let's call that variable $p_1 := \operatorname{argmax}_p |a_p|$. Subsequently, if p_1 is more than twice the size of the second largest coefficient $p_2 := \operatorname{argmax}_{p \neq p_1} |a_p|$, the second split in each of the two leaves will occur along variable p_1 as well. Otherwise, it will occur along variable p_2 . Under our large sample assumptions, all the nodes at a given depth will behave uniformly, splitting alternatively along variables until the terms $|a_p|(u_p - l_p)$ are within a multiple of two of one another. Denote the index of the minimum coefficient as $p^\wedge := \operatorname{argmin}_p |a_p|$ and assume for now that a_{p^\wedge} is nonzero. Using the notation $\lfloor c \rfloor$ to denote the integer part of c , the number of iterations in this first stage is thus given by

$$\sum_{p \neq p^\wedge} \lfloor \log_2 \frac{|a_p|}{|a_{p^\wedge}|} \rfloor \leq (P - 1) \log_2 \frac{|a_{p_1}|}{|a_{p^\wedge}|}. \quad (7)$$

Subsequently, in the second phase, the algorithm will subdivide boxes by proceeding alternatively through the variables one by one *ad infinitum*. If one or more a_p is zero, the analysis above can be applied on the nonzero parameters. This reduces the number of iterations until the first phase concludes and the second starts below $\|\mathbf{a}\|_0 \log_2 \frac{\max_p |a_p|}{\min_{\{p: a_p \neq 0\}} |a_p|}$.

¹Namely $C_i^l(t, s) = \prod_{p < s} [l_{i,p}, u_{i,p}] \times [l_{i,s}, t] \times \prod_{p > s} [l_{i,p}, u_{i,p}]$ and $C_i^r(t, s) = \prod_{p < s} [l_{i,p}, u_{i,p}] \times [t, u_{i,s}] \times \prod_{p > s} [l_{i,p}, u_{i,p}]$

3.2 An Average Difference Estimator for Generic Trees

Independently of how the tree was formed, by a greedy mechanism or a different one, if node i splits along variable σ_i , then we can build an estimate of a_{σ_i} by comparing the values of its children $v_{C_i^l}$ and $v_{C_i^r}$. Since $\mathbb{E}[v_i] = \mathbb{E}[\mathbf{a}^\top \mathbf{x} + b; [\mathbf{l}_i, \mathbf{u}_i]] = \sum_p a_p \frac{u_{p,i} + l_{p,i}}{2} + b$, we have that

$$\mathbb{E}[v_{C_i^l}] = \sum_{p \neq \sigma_i} a_p \frac{u_p + l_p}{2} + a_{\sigma_i} \frac{\tau_i + l_{i,p}}{2} + b; \quad \mathbb{E}[v_{C_i^r}] = \sum_{p \neq \sigma_i} a_p \frac{u_p + l_p}{2} + a_{\sigma_i} \frac{u_{i,p} + \tau_i}{2} + b, \quad (8)$$

and thus we can develop the following unbiased estimate for a_{σ_i} :

$$\mathbb{E} \left[\frac{2(v_{C_i^r} - v_{C_i^l})}{u_{i,\sigma_i} - l_{i,\sigma_i}} \right] = a_{\sigma_i}. \quad (9)$$

This suggests the following algorithm for extracting linear coefficients from regression trees.

Algorithm 1 Unbiased Linear Function Estimation with Trees

Require: $n \geq 0$
Ensure: $y = x^n$

```

Gi  $\leftarrow \mathbf{0}_P$  for all  $i$ .
for  $k \in \{1, \dots, K\}$  do
  for  $i \in \mathcal{D}_k$  do
    Gi,si  $\leftarrow \frac{2(v_{C_i^r} - v_{C_i^l})}{u_{C_i^r} - l_{C_i^l}}$  ▷ Update estimate of a along split direction.
    GCir,:, GCil,:  $\leftarrow \mathbf{G}_{i,:}$  ▷ Propagate gradient estimate to child nodes.
  end for
end for

```

We can see that once each feature has been iterated over once, \mathbf{G}_i will be an unbiased estimator of \mathbf{a} . Furthermore, in the large data limit, the analysis of the previous section reveals that this will occur within $(P-1) \log_2 \left(\frac{\max_p |a_p|}{\min_p |a_p|} \right)$ splits. This suggests that depth should grow linearly with dimension, or least with the number of nonzero coefficients in the gradient.

4 Estimating and Integrating Gradients

In this section, we will put to work the simple iteration developed in the previous section to estimate gradient-based quantities. Denote $r_k := \max_{i \in \mathcal{D}_k} \text{diam}(\mathcal{N}_i) = \max_{i \in \mathcal{D}_k} \|\mathbf{u}_i - \mathbf{l}_i\|_1$ which gives the maximum diameter of any node of depth k . The analytic strategy in this section will be to consider trees estimating continuously differentiable functions for which $r_k \rightarrow 0$. In such circumstances, once the nodes are of sufficiently small diameter, a series expansion will allow us to treat the function as nearly linear on each node, and the technology developed in the previous section will allow us to produce gradient estimates. Proofs are presented in Appendix A.

Our main result is says that as the depth of the tree grows and the sample size increases, the linear coefficient estimates of the previous section converge to the gradient at any point $\mathbf{x} \in [0, 1]^P$.

Proposition 1. *Let G be produced according to Algorithm 1 applied to a greedily estimated regression tree fit to data with finite variance fit to a function f continuously differentiable on $[0, 1]^P$. Then, for all $\mathbf{x} \in [0, 1]^P$,*

$$\lim_{k \rightarrow \infty} \lim_{N \rightarrow \infty} G_{B^k(\mathbf{x})} = \nabla f(\mathbf{x}). \quad (10)$$

Now that we have the ability to estimate gradients at any individual point in the space, the remainder of this section will develop the asymptotics of tree-based estimates of existing gradient-based sensitivity and interpretability quantities.

We begin with two strategies for estimating the active subspace matrix using our proposed gradient estimator. First, we develop an estimator derived via weighted summation over leaf node gradient estimates.

Corollary 1. *Let G be produced according to Algorithm 1 applied to a greedily estimated regression tree fit to data with finite variance fit to a function f continuously differentiable on $[0, 1]^P$ whose gradient is integrable with respect to μ . Then,*

$$\lim_{k \rightarrow \infty} \lim_{N \rightarrow \infty} \sum_{i \in \mathcal{D}_k} \mathbf{G}_i \mathbf{G}_i^\top \mu(\mathcal{N}_i) = \int_{[0,1]^P} \nabla f(\mathbf{x}) \nabla f(\mathbf{x}) d\mu(\mathbf{x}). \quad (11)$$

Therefore, regression trees, like Gaussian processes but unlike neural networks, have a deterministic, “closed form” estimator for the active subspace available. This approach does not depend on Lebesgue continuity, but rather can be applied to any measure defined on rectangles. However, for some measures in high dimension, it is difficult to compute the measure of an arbitrary rectangle. Therefore, we also consider a “Monte-Carlo over surrogate” approach to estimating the active subspace, which will allow the use of any measure which can be efficiently sampled from.

Corollary 2. *Let G and f be as in Corollary 1. Then,*

$$\lim_{k, N, M \rightarrow \infty} \frac{1}{M} \sum_{\mathbf{x}_m \sim \mu} \mathbf{G}_{B^k(\mathbf{x}_m)} \mathbf{G}_{B^k(\mathbf{x}_m)}^\top = \int_{[0,1]^P} \nabla f(\mathbf{x}) \nabla f(\mathbf{x}) d\mu(\mathbf{x}). \quad (12)$$

Finally, we also develop a tree-based method for local interpretation by studying a sequence of quantities which converges to the Integrated Gradient.

Corollary 3. *Let G be produced according to Algorithm 1 applied to a greedily estimated regression tree fit to data with finite variance fit to a function f continuously differentiable on $[0, 1]^P$ whose gradient is integrable with respect to the Lebesgue measure. Then,*

$$\lim_{k, N, M \rightarrow \infty} (\mathbf{x} - \mathbf{x}^*) \odot \frac{1}{M} \sum_{m=1}^M G_{B^k(\alpha_m \mathbf{x} + (1 - \alpha_m) \mathbf{x}^*)} = (\mathbf{x} - \mathbf{x}^*) \odot \int_{\alpha=0}^1 \nabla f(\alpha \mathbf{x} + (1 - \alpha) \mathbf{x}^*) d\alpha \quad (13)$$

We have thus established consistency of gradient-based model interpretation quantities for regression trees. Next, we will empirically study their behavior in finite samples via a battery of numerical experiments.

5 Numerical Experiments

We now study how the proposed gradient estimator might be profitably exploited in practice. We begin with three quantitative studies, first investigating the potential of a tree-estimated active subspace to improve prediction accuracy of a downstream tree via a rotation of the space. Subsequently, we evaluate the capacity of regression trees to estimate the Active Subspace in low and high dimension. On these problems, we use the estimator of Corollary 1, which we term the Tree-Based Active Subspace (TBAS) estimator. Finally, we conduct two qualitative studies, one demonstrating how a TBAS can provide data visualization, and one showing how a tree-estimated integrated gradient can facilitate local model interpretation.

5.1 Active-subspace Rotated Trees

This section evaluates the ability of TBAS to improve the accuracy of a downstream predictive analysis. Given some mapping \mathbf{L} , we refer to postmultiplication of the feature matrix \mathbf{X} to form a new feature matrix $\mathbf{Z} := \mathbf{XL}$ as a rotation. In standard tree-based methods, non-diagonal rotations can have an impact on predictive performance because the axes along which splits are made have been changed. In order to quantitatively assess the utility of TBAS, we compare the prediction error of regression trees and random forests on eight benchmark datasets fit on data augmented by a rotation of the space. We compare TBAS rotations to those made by drawing orthogonal directions uniformly over the Grassmannian (Rand; similar to (Breiman, 2001, Section 5)) as well as those formed from a Principal Components Analysis (PCA; similar to Rodriguez et al. (2006)) and no rotation at all (Id). Table 1 presents the results of this analysis. TBAS does at least as well as the other methods, and sometimes offers significant improvement (such as on the Kin40k and Keggu datasets).

Dataset:	bike	concrete	gas	grid	keggu	kin40k	obesity	supercond
Regression Tree (Depth 4)								
TBAS	0.635	0.47	0.578	0.688	0.194	0.856	0.128	0.511
Id	0.655	0.537	0.595	0.773	0.35	0.963	0.226	0.514
PCA	0.655	0.543	0.591	0.773	0.349	0.964	0.226	0.513
Rand	0.656	0.524	0.593	0.752	0.349	0.95	0.226	0.513
Regression Tree (Depth 8)								
TBAS	0.402	0.35	0.429	0.521	0.078	0.586	0.094	0.392
Id	0.405	0.403	0.432	0.522	0.121	0.862	0.103	0.395
PCA	0.407	0.395	0.423	0.524	0.122	0.872	0.107	0.392
Rand	0.411	0.391	0.435	0.55	0.124	0.836	0.109	0.397
Random Forest (Depth 4)								
TBAS	0.609	0.406	0.559	0.602	0.161	0.802	0.123	0.479
Id	0.65	0.462	0.574	0.659	0.344	0.954	0.173	0.485
PCA	0.649	0.462	0.567	0.654	0.344	0.954	0.174	0.486
Rand	0.646	0.458	0.57	0.66	0.33	0.938	0.173	0.486

Table 1: **Predictive Impact of Various Transformations on Selected Datasets.** Numbers give 100-fold RMSE; bold indicates confidence interval overlaps with the lowest confidence interval.

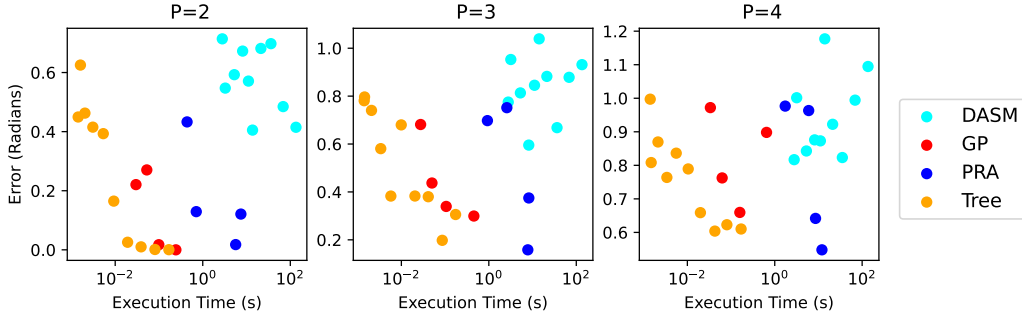


Figure 2: **Active Subspace Estimation in Low Dimension.** Execution time (x-axis) and Subspace Estimation Error (y-axis) for the four methods, lower is better.

5.2 Computationally Efficient Active Subspace Estimation in Low Dimension

In this section we demonstrate the capability of TBAS to offer extremely fast, gradient-free estimation of the active subspace in low dimension when significant data are available. We compare to the three popular methods for gradient-free active subspace estimation introduced in Section 2.2, based on a Gaussian Process (GP), Ridge Polynomial (PRA), and Neural Network (DASM). Each of these methods was tasked to estimate a one dimensional active subspace in dimensions 2, 3 and 4, using a logarithmically spaced grid of sample sizes ranging from 10 to 10,000 on a toy algebraic function. We found that the GP and PRA methods worked efficiently when sample sizes were small, but computation time grew quickly, such that we were only able to run these methods for samples of size 150 or less. Figure 2 shows the active subspace error against the execution time. We see that the tree-based estimator forms the majority of the Pareto front in all three cases.

5.3 Estimating Sparse Active Subspaces in High Dimension

Imposing sparsity in the coefficients of linear dimension reduction can improve interpretability (Zou et al., 2006). Because of the manner that tree-based methods produce gradient estimates, we conjecture that TBAS has built-in inductive bias to favor entry-wise active subspaces. Our analysis in Section 3.1 revealed that in the large sample limit, the tree-based gradient estimator will behave as

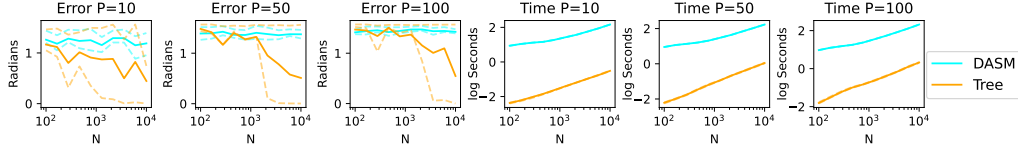


Figure 3: **Sparse Active Subspace Estimation in High Dimension.** Lower is better.

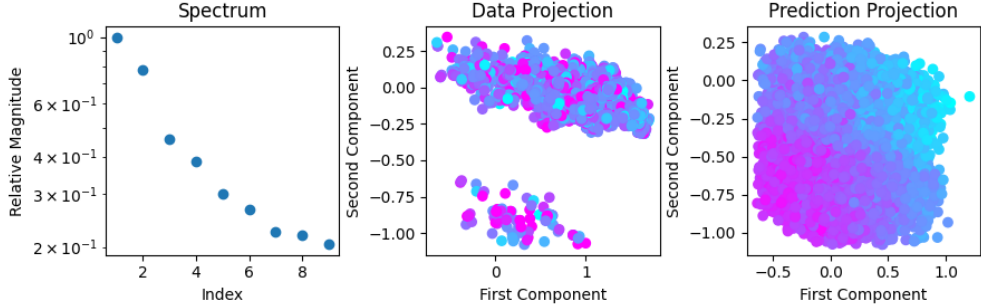


Figure 4: **Projection with TBAS.** *Left:* Spectrum of active subspace matrix suggests a 2D active subspace. *Middle:* Projection of data onto active subspace. *Left:* Projection of predictive surface.

though it was in a lower dimensional space, with dimension given by the cardinality of the gradient. In this section, we will investigate this property by comparing TBAS against the DASM in estimating a sparse active subspace in dimensions 10, 50 and 100. We will use the same setup as the previous section, except that the true subspace has only three nonzero coordinates. Because of the sample size that is required to estimate an active subspace in high dimension, it is computationally infeasible to deploy the GP or PRA active subspace estimation methods. Figure 3 shows the results of this analysis. The TBAS estimator is able to achieve much better accuracy with a significantly smaller cost,

5.4 Dimension Reduction with the Active Subspace

We now turn to the qualitative benefits of performing an active subspace analysis using TBAS. We used the NHEFS dataset of biochemistry tape and mortality data which were used by Lundberg et al. (2019). This consisted of a dataset of 14,407 observations and 90 complete variables. We fit a TBAS to this dataset using a regression tree of depth 15, requiring at least 10 samples per leaf. We subsequently performed an eigendecomposition of the estimated active subspace matrix. Like (Lundberg et al., 2019), we found that age was the most important variable and it mapped cleanly onto the first active subspace dimension. However, we found that the next two dimensions consisted of many variables (see Appendix B.3). Figure 4 shows there result of this analysis, which reveals that after Age there appears to be a gap in the spectrum of the active subspace matrix (Constantine, 2015), indicating the presence of an active subspace of dimension two (left panel). The middle panel shows a projection of the data, which breaks into two clusters along the second principal component, while the right panel shows a projection of randomly sampled points to visualize the predictive surface of the function. The right panel reveals the predictive surface has a fairly simple, “S-shaped” form over these two dimension. It would not be possible to detect this by considering only main effects or two factor interactions.

5.5 Integrated Gradient for Tree-Based Methods

We now consider random forest classifier fit the to two subsets of the MNIST dataset, one contrasting zeros against eights and the other fours against sevens. While classification was not the focus of this article, we present some preliminary numerical experiments in Appendix C. We use the estimator suggested by Corollary 3 with $M = 500$ points along a given path. Figure 5 gives the results of this analysis. We see that when comparing eights against zeros, the intersection point of the eight is most important, while the left and right sides of the zero are. This makes sense as they are the parts of each

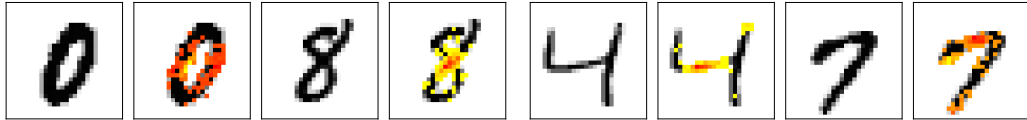


Figure 5: **Integrated Gradient for Trees.** Each pair of panels gives a training example from MNIST. The second pair in the image superimposes the IG values onto the example. Redder means more strongly suggesting correct class membership.

digit which are distinct. By contrast, the shared upper and lower arcs are not highlighted. In the four versus seven case, the location of the horizontal bar seems to be most influential in determining one versus the other. This suggests that the model is comparing the relative position of the bar to the rest of the digit in making its classifications.

6 Discussion

Summary: We proposed a simple method for estimating gradients in sufficiently deep regression trees on large datasets. Subsequently, we demonstrate how these estimates could be used to calculate active subspaces and integrated gradients. We found significant improvement in predictive performance could be achieved by using the tree-based active subspace to rotate the space, and also found that these estimates executed quicker than existing gradient-free active subspace estimators and had useful inductive bias towards detecting coordinate-sparse subspaces. Also, we were not able to run the PRA and GP based active subspace estimators on larger datasets due to computational constraints. Finally, we used these gradient estimates to reveal the simple global structure of a tree-based model fit to a complex dataset as well as the mechanism by which a random forest conducted MNIST classification.

Limitations: When it comes to limitations of our experiments, when comparing our active subspace estimates to the DASM, we used a particular neural network architecture and optimizer. It is possible that a different configuration would have performed better. Additionally, when it comes to limitations of the method, our analysis suggests that it would take a very deep regression tree to estimate gradients in high dimension if the gradient is dense in all of its entries.

Conclusions: We think this work offers two high level conclusions. First, that trees may have a place in the field of Uncertainty Quantification, which has more commonly used differentiable but slow to estimate surrogates such as Gaussian processes and neural networks. Secondly, we hope that this work can also enable improve cross-pollination between developments in interpretability for neural networks and for regression trees by creating analogs for gradient-based neural network techniques.

We also would like to comment on how TBAS fit into the existing literature on interpretability in trees. It is somewhat distinct from the axiomatic approach to interpretability proffered by SHAP (Lundberg and Lee, 2017) and Integrated Gradients (Sundararajan et al., 2017). While an axiomatic approach can be useful, its universality should not be exaggerated. Hancox-Li and Kumar (2021) write about how it is unlikely that any variable selection method could satisfy all possible demands, no matter how attractive its axiomatic foundation. Since the active subspace is parameterized by a measure, it actually consists of an entire family of analyses, with different choices of emphasis over the input space possibly leading to different conclusions.

Future Work: We are excited about the future work opened up by the here-proposed gradient estimates. First, while we have conducted some preliminary analyses in Appendix C, more work is needed to understand the properties of these estimates in classification problems with categorical inputs and missing data. We are also interested in the possibility of estimating higher order derivatives from tree structure. Furthermore, extending the class of functions approximated to nondifferentiable functions is of interest: does the quantity proposed here converge in such a case, and to what? But we are most excited about the potential to bring in other gradient-based techniques to tree-based methods. For instance, physic-informed machine learning (e.g. Raissi et al. (2019, 2017)) has been making waves in the fluid dynamics community (Cai et al., 2021) among other applications, where they allow the analyst to use information about function derivatives to improve predictions of differentiable models such as neural networks or Gaussian processes. Our gradient estimator may allow this approach to be deployed on regression trees.

References

Bradbury, J., Frostig, R., Hawkins, P., Johnson, M. J., Leary, C., Maclaurin, D., Necula, G., Paszke, A., VanderPlas, J., Wanderman-Milne, S., and Zhang, Q. (2018). JAX: composable transformations of Python+NumPy programs.

Breiman, L. (2001). Random forests. *Machine learning*, 45:5–32.

Breiman, L. (2002). Manual on setting up, using, and understanding random forests v3. 1. *Statistics Department University of California Berkeley, CA, USA*, 1(58):3–42.

Breiman, L. (2017). *Classification and regression trees*. Routledge.

Cai, S., Mao, Z., Wang, Z., Yin, M., and Karniadakis, G. E. (2021). Physics-informed neural networks (pinns) for fluid mechanics: A review. *Acta Mechanica Sinica*, 37(12):1727–1738.

Chaudhuri, P., Lo, W.-D., Loh, W.-Y., and Yang, C.-C. (1995). Generalized regression trees. *Statistica Sinica*, pages 641–666.

Chen, H., Janizek, J. D., Lundberg, S., and Lee, S.-I. (2020). True to the model or true to the data? *arXiv preprint arXiv:2006.16234*.

Constantine, P. G. (2015). *Active subspaces: Emerging ideas for dimension reduction in parameter studies*. SIAM.

Edeling, W. (2023). On the deep active-subspace method. *SIAM/ASA Journal on Uncertainty Quantification*, 11(1):62–90.

Friedman, J. H. (2001). Greedy function approximation: a gradient boosting machine. *Annals of statistics*, pages 1189–1232.

Hancox-Li, L. and Kumar, I. E. (2021). Epistemic values in feature importance methods: Lessons from feminist epistemology. In *proceedings of the 2021 ACM conference on fairness, accountability, and transparency*, pages 817–826.

Hechtlinger, Y. (2016). Interpretation of prediction models using the input gradient. *arXiv preprint arXiv:1611.07634*.

Hokanson, J. M. and Constantine, P. G. (2018). Data-driven polynomial ridge approximation using variable projection. *SIAM Journal on Scientific Computing*, 40(3):A1566–A1589.

Hooker, G., Mentch, L., and Zhou, S. (2021). Unrestricted permutation forces extrapolation: variable importance requires at least one more model, or there is no free variable importance. *Statistics and Computing*, 31:1–16.

Ishwaran, H. (2007). Variable importance in binary regression trees and forests.

Karczmarz, A., Michalak, T., Mukherjee, A., Sankowski, P., and Wygocki, P. (2022). Improved feature importance computation for tree models based on the banzhaf value. In *Uncertainty in Artificial Intelligence*, pages 969–979. PMLR.

Kazemitabar, J., Amini, A., Bloniarz, A., and Talwalkar, A. S. (2017). Variable importance using decision trees. *Advances in neural information processing systems*, 30.

Klusowski, J. M. and Tian, P. M. (2020). Nonparametric variable screening with optimal decision stumps. *arXiv preprint arXiv:2011.02683*.

Li, X., Wang, Y., Basu, S., Kumbier, K., and Yu, B. (2019). A debiased mdi feature importance measure for random forests. *Advances in Neural Information Processing Systems*, 32.

Loh, W.-Y. (2011). Classification and regression trees. *Wiley interdisciplinary reviews: data mining and knowledge discovery*, 1(1):14–23.

Louppe, G. (2014). Understanding random forests: From theory to practice. *arXiv preprint arXiv:1407.7502*.

Louppe, G., Wehenkel, L., Sutera, A., and Geurts, P. (2013). Understanding variable importances in forests of randomized trees. *Advances in neural information processing systems*, 26.

Lundberg, S. M., Erion, G., Chen, H., DeGrave, A., Prutkin, J. M., Nair, B., Katz, R., Himmelfarb, J., Bansal, N., and Lee, S.-I. (2019). Explainable ai for trees: From local explanations to global understanding. *arXiv preprint arXiv:1905.04610*.

Lundberg, S. M. and Lee, S.-I. (2017). A unified approach to interpreting model predictions. *Advances in neural information processing systems*, 30.

McCloskey, K., Taly, A., Monti, F., Brenner, M. P., and Colwell, L. J. (2019). Using attribution to decode binding mechanism in neural network models for chemistry. *Proceedings of the National Academy of Sciences*, 116(24):11624–11629.

Pedregosa, F., Varoquaux, G., Gramfort, A., Michel, V., Thirion, B., Grisel, O., Blondel, M., Prettenhofer, P., Weiss, R., Dubourg, V., Vanderplas, J., Passos, A., Cournapeau, D., Brucher, M., Perrot, M., and Duchesnay, E. (2011). Scikit-learn: Machine learning in Python. *Journal of Machine Learning Research*, 12:2825–2830.

Raissi, M., Perdikaris, P., and Karniadakis, G. E. (2017). Machine learning of linear differential equations using gaussian processes. *Journal of Computational Physics*, 348:683–693.

Raissi, M., Wang, Z., Triantafyllou, M. S., and Karniadakis, G. E. (2019). Deep learning of vortex-induced vibrations. *Journal of Fluid Mechanics*, 861:119–137.

Rodriguez, J. J., Kuncheva, L. I., and Alonso, C. J. (2006). Rotation forest: A new classifier ensemble method. *IEEE transactions on pattern analysis and machine intelligence*, 28(10):1619–1630.

Sandri, M. and Zuccolotto, P. (2008). A bias correction algorithm for the gini variable importance measure in classification trees. *Journal of Computational and Graphical Statistics*, 17(3):611–628.

Sayres, R., Taly, A., Rahimy, E., Blumer, K., Coz, D., Hammel, N., Krause, J., Narayanaswamy, A., Rastegar, Z., Wu, D., et al. (2019). Using a deep learning algorithm and integrated gradients explanation to assist grading for diabetic retinopathy. *Ophthalmology*, 126(4):552–564.

Shan, H., Zhang, J., and Kruger, U. (2015). Learning linear representation of space partitioning trees based on unsupervised kernel dimension reduction. *IEEE Transactions on Cybernetics*, 46(12):3427–3438.

Strobl, C., Boulesteix, A.-L., Kneib, T., Augustin, T., and Zeileis, A. (2008). Conditional variable importance for random forests. *BMC bioinformatics*, 9:1–11.

Strobl, C., Boulesteix, A.-L., Zeileis, A., and Hothorn, T. (2007). Bias in random forest variable importance measures: Illustrations, sources and a solution. *BMC bioinformatics*, 8:1–21.

Sundararajan, M., Taly, A., and Yan, Q. (2017). Axiomatic attribution for deep networks. In *International conference on machine learning*, pages 3319–3328. PMLR.

Tripathy, R. and Bilionis, I. (2019). Deep active subspaces: A scalable method for high-dimensional uncertainty propagation. In *International Design Engineering Technical Conferences and Computers and Information in Engineering Conference*, volume 59179, page V001T02A074. American Society of Mechanical Engineers.

Wycoff, N., Binois, M., and Wild, S. M. (2021). Sequential learning of active subspaces. *Journal of Computational and Graphical Statistics*, 30(4):1224–1237.

Zou, H., Hastie, T., and Tibshirani, R. (2006). Sparse principal component analysis. *Journal of computational and graphical statistics*, 15(2):265–286.

A Proofs

Proposition 1. Let G be produced according to Algorithm 1 applied to a greedily estimated regression tree fit to data with finite variance fit to a function f continuously differentiable on $[0, 1]^P$. Then, for all $\mathbf{x} \in [0, 1]^P$,

$$\lim_{k \rightarrow \infty} \lim_{N \rightarrow \infty} G_{B^k(\mathbf{x})} = \nabla f(\mathbf{x}). \quad (14)$$

Proof. Denote by \mathbf{x}^* the point at which we wish to estimate the gradient. This proof will proceed in two parts, each analogous to a subsection of Section 3.

First, we will show that the difference between values at the leaf nodes can be used to asymptotically unbiasedly estimate the gradient. Second, we will show that the iteration between which variables are split will eventually look like that when estimating a linear function.

Consider a nested sequence of trees of depth k . For each k , denote by $i^k \in \mathbb{N}^+$ the index of the leaf node containing \mathbf{x}^* .

Expand $f(\mathbf{x})$ about \mathbf{x}^* :

$$f(\mathbf{x}) = f(\mathbf{x}^*) + \nabla f(\mathbf{x}^*)^\top (\mathbf{x} - \mathbf{x}^*) + o(\|\mathbf{x} - \mathbf{x}^*\|_2) \quad (15)$$

Then we have that:

$$\mathbb{E}_{\mathbf{x} \sim U[\mathbf{l}, \mathbf{u}]}[f(\mathbf{x})] = f(\mathbf{x}^*) + \nabla f(\mathbf{x}^*)^\top \left(\frac{\mathbf{u} + \mathbf{l}}{2} - \mathbf{x}^* \right) + o(r_k) \quad (16)$$

Since $\lim_{N \rightarrow \infty} v_j = \mathbb{E}_{\mathbf{x} \sim U[\mathbf{l}_j, \mathbf{u}_j]}[f(\mathbf{x})]$ for all j ,

$$\lim_{N \rightarrow \infty} v_{\mathbf{C}_{i^k}^r} - v_{\mathbf{C}_{i^k}^l} = \nabla f(\mathbf{x}^*)^\top \left(\frac{\mathbf{u}_{\mathbf{C}_{i^k}^r} + \mathbf{l}_{\mathbf{C}_{i^k}^r}}{2} - \frac{\mathbf{u}_{\mathbf{C}_{i^k}^l} + \mathbf{l}_{\mathbf{C}_{i^k}^l}}{2} \right) + o(r_k) \quad (17)$$

$$= \frac{f(\mathbf{x}^*)}{\partial x_{s_{i^k}}} \frac{(u_{i^k, s_{i^k}} - l_{i^k, s_{i^k}})}{4} + o(r_k). \quad (18)$$

This will converge to the gradient so long as the diameter of the maximum node converges to zero. So we have shown that the difference in child leaf node values can be used to estimate the elements of the gradient vector, provided that we iterate over all nodes infinitely often.

As we noted in Section 3, the variable which will be split at each iteration is that variable s which minimizes:

$$\min_{t \in [l_{i,s}, u_{i,s}]} \mathbb{V}[f(\mathbf{x}); C_i^l(t, s)] + \mathbb{V}[f(\mathbf{x}); C_i^r(t, s)] \quad (19)$$

Using our series expansion, we may write:

$$\mathbb{V}[f(\mathbf{x}); C_i^l(t, s)] \quad (20)$$

$$= \mathbb{V}[\nabla f(\mathbf{x}^*)^\top \mathbf{x}; C_i^l(t, s)] + 2\mathbb{V}[\nabla f(\mathbf{x}^*)^\top \mathbf{x}, o(r^k); C_i^l(t, s)] + \mathbb{V}[o(r^k); C_i^l(t, s)] \quad (21)$$

$$= \mathbb{V}[\nabla f(\mathbf{x}^*)^\top \mathbf{x}; C_i^l(t, s)] + o(r^k) \quad (22)$$

Consequently, so long as r^k is sufficiently small, then the little o term will be less than the minimum element of $\nabla f(\mathbf{x}^*)$, and the iteration will eventually alternate between all variables.

□

Corollary 1. Let G be produced according to Algorithm 1 applied to a greedily estimated regression tree fit to data with finite variance fit to a function f continuously differentiable on $[0, 1]^P$ whose gradient is integrable with respect to μ . Then,

$$\lim_{k \rightarrow \infty} \lim_{N \rightarrow \infty} \sum_{i \in \mathcal{D}_k} \mathbf{G}_i \mathbf{G}_i^\top \mu(\mathcal{N}_i) = \int_{[0, 1]^P} \nabla f(\mathbf{x}) \nabla f(\mathbf{x}) d\mu(\mathbf{x}). \quad (23)$$

Proof. Since the function sequence $\mathbf{g}^k(\mathbf{x}) := G_{B^k(\mathbf{x})}$ converges pointwise to $\nabla f(\mathbf{x})$ by Proposition 1, we need only establish a function $H(\mathbf{x})$ which dominates $\mathbf{g}^k(\mathbf{x})$ and apply the Dominated Convergence Theorem.

To this end, examine the gradient estimator of node i 's p th entry, given by:

$$\frac{2(v_{C_i^r} - v_{C_i^l})}{u_{p,i} - l_{p,i}} = \frac{2\left(\frac{1}{|\mathcal{N}_{C_i^r}|} \int_{\mathcal{N}_{C_i^r}} f(\mathbf{x}) d\mathbf{x} - \frac{1}{|\mathcal{N}_{C_i^l}|} \int_{\mathcal{N}_{C_i^l}} f(\mathbf{x}) d\mathbf{x}\right)}{u_{p,i} - l_{p,i}}. \quad (24)$$

The magnitude of this difference in averages is bounded by the magnitude of the difference of extremes:

$$\left| \frac{1}{|\mathcal{N}_{C_i^r}|} \int_{\mathcal{N}_{C_i^r}} f(\mathbf{x}) d\mathbf{x} - \frac{1}{|\mathcal{N}_{C_i^l}|} \int_{\mathcal{N}_{C_i^l}} f(\mathbf{x}) d\mathbf{x} \right| \leq \max_{(\mathbf{x}_1, \mathbf{x}_2) \in \mathcal{N}_{C_i^r} \times \mathcal{N}_{C_i^l}} |f(\mathbf{x}_1) - f(\mathbf{x}_2)| \quad (25)$$

But since f is continuously differentiable, it is also Lipschitz continuous (call the constant L), and we have that:

$$\max_{(\mathbf{x}_1, \mathbf{x}_2) \in \mathcal{N}_{C_i^r} \times \mathcal{N}_{C_i^l}} |f(\mathbf{x}_1) - f(\mathbf{x}_2)| \leq L \|\mathbf{x}_1 - \mathbf{x}_2\|_2 \leq PL \|\mathbf{x}_1 - \mathbf{x}_2\|_\infty. \quad (26)$$

Therefore:

$$\left| \frac{2(v_{C_i^r} - v_{C_i^l})}{u_{p,i} - l_{p,i}} \right| \leq \left| \frac{2(PL \|\mathbf{x}_1 - \mathbf{x}_2\|_\infty)}{u_{p,i} - l_{p,i}} \right| \leq 2PL. \quad (27)$$

Hence the constant $2PL$ bounds $g^k(\mathbf{x})$, and thence $4P^2L^2$ bounds the outer product function. Since the integral is over the unit hypercube, the constant function is integrable and we can apply the Dominated Convergence Theorem to yield the desired result. \square

Corollary 2. *Let G and f be as in Corollary 1. Then,*

$$\lim_{k, N, M \rightarrow \infty} \frac{1}{M} \sum_{\mathbf{x}_m \sim \mu} \mathbf{G}_{B^k(\mathbf{x}_m)} \mathbf{G}_{B^k(\mathbf{x}_m)}^\top = \int_{[0,1]^P} \nabla f(\mathbf{x}) \nabla f(\mathbf{x}) d\mu(\mathbf{x}). \quad (28)$$

Proof. This follows from the fact that

$$\lim_{M \rightarrow \infty} \frac{1}{M} \sum_{\mathbf{x}_m \sim \mu} \mathbf{G}_{B^k(\mathbf{x}_m)} \mathbf{G}_{B^k(\mathbf{x}_m)}^\top = \int_{\mathbf{x} \in [0,1]^P} \mathbf{G}_{B^k(\mathbf{x})} \mathbf{G}_{B^k(\mathbf{x})}^\top d\mu = \sum_{i \in \mathcal{D}_k} \mathbf{G}_i \mathbf{G}_i^\top \mu(\mathcal{N}_i) \quad (29)$$

and an application of Corollary 1. \square

Corollary 3. *Let G be produced according to Algorithm 1 applied to a greedily estimated regression tree fit to data with finite variance fit to a function f continuously differentiable on $[0, 1]^P$ whose gradient is integrable with respect to the Lebesgue measure. Then,*

$$\lim_{k, N, M \rightarrow \infty} (\mathbf{x} - \mathbf{x}^*) \odot \frac{1}{M} \sum_{m=1}^M G_{B^k(\alpha_m \mathbf{x} + (1 - \alpha_m) \mathbf{x}^*)} = (\mathbf{x} - \mathbf{x}^*) \odot \int_{\alpha=0}^1 \nabla f(\alpha \mathbf{x} + (1 - \alpha) \mathbf{x}^*) d\alpha \quad (30)$$

Proof. Similarly as the proof of Corollary 2, we begin with

$$\lim_{M \rightarrow \infty} \sum_{m=1}^M G_{B^k(\alpha_m \mathbf{x} + (1 - \alpha_m) \mathbf{x}^*)} = \int_{\alpha=0}^1 G_{B^k(\alpha \mathbf{x} + (1 - \alpha) \mathbf{x}^*)} d\alpha \quad (31)$$

Subsequently, we can use the Dominated Convergence Theorem again as in the proof of Proposition 1 using the same dominating function developed therein. \square

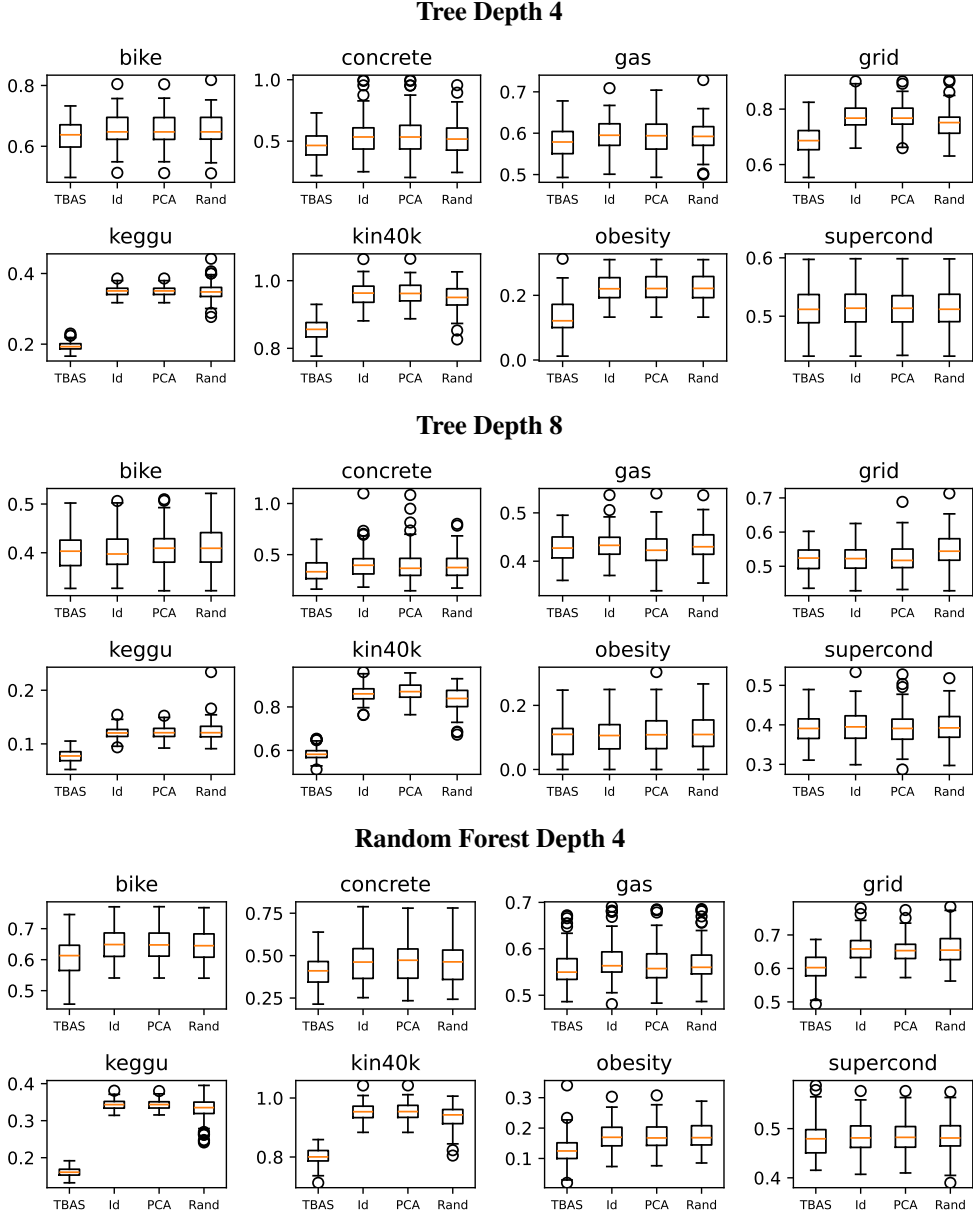


Figure 6: Boxplots corresponding to Table 1.

B Details of Numerical Experiments

This section gives additional details and discussion of the numerical results presented in Section 5. All tree-based models are estimated using Scikit-Learn Pedregosa et al. (2011).

B.1 Rotation Prediction Study Additional Details

In this study, when performing a rotation, we used only the \sqrt{P} many PCA components or Active Subspace dimensions, and appended these to the original design matrix as new variables. We measure prediction error using 100-fold cross validation.

The table below gives the parameters of the datasets used for the prediction study of Section 5.1.

Name	N	P	URL
concrete	1,030	9	https://archive.ics.uci.edu/dataset/165/
kin40k	40,000	9	https://github.com/alshedivat/keras-gp/kgp/datasets/kin40k.py
kegg	65,554	28	https://www.genome.jp/kegg/pathway.html
bike	17,379	13	https://archive.ics.uci.edu/dataset/560/
obesity	2,111	24	https://archive.ics.uci.edu/dataset/544/
gas	36,733	12	https://archive.ics.uci.edu/dataset/224
grid	10,000	13	https://archive.ics.uci.edu/dataset/471/
supercond	21,263	82	https://archive.ics.uci.edu/dataset/464/

We also provide boxplots of Cross Validation errors in Figure 6. Running this study took about five hours on a 40 core Ubuntu machine with 128 GB of RAM.

B.2 Active Subspace Estimation Study Additional Details

In Section 5.2, We randomly sampled a unit vector \mathbf{a} from the uniform distribution over directions and then sampled input points uniformly at random on the unit cube. We subsequently evaluated the function $f(\mathbf{x}) = \cos(6\pi(\mathbf{a}^\top(\mathbf{x} - 0.5)))$ which was treated as the noiseless observed response \mathbf{y} . We compared the estimates with using the angle each made with \mathbf{a} . This experiment was repeated 20 times.

We used the implementation of PRA provided with the pypi package PSDR². For GP-based active subspace estimation, we used the CRAN package activegp. We used all default settings for the PRA method as well as for the GP method. For the DASM, we used a neural network with an additional layer of width 512 subsequent to the active subspace layer, and used gradient descent with a step size of 10^{-3} on the Mean Squared Error cost function. This neural network was implemented in JAX Bradbury et al. (2018). In addition to the quantitative advantages enjoyed by the tree-based method of active subspace estimation, we would also like to note that like the GP-based method, and unlike the PRA and DASM, it provides an estimate of the entire active subspace matrix, rather than simply a basis for the active subspace. This is important for two reasons. First, with the active subspace matrix in hand, we can create analogs of PCA scree plots to determine what dimension of the active subspace is most desirable, or to get some idea of how much information is being lost in, say, a two dimensional visualization. And secondly, it allows us to decide on an active subspace dimension *after* having seen the data rather than before, without requiring the estimation procedure to be re-run.

Running this study took about eight hours on a 40 core Ubuntu machine with 128 GB of RAM.

B.3 NHEFS Data Analysis Details

This table presents the first 3 eigenvectors of the mortality data analysis, restricting to the top 9 variables with highest coefficients. The first eigenvector captures almost entirely the age variable, which Lundberg et al. (2019) also found to be most important. We see that the second eigenvector is evenly distributed across sex and one of the urine variables. The third eigenvector is dominated by the urineDark variable.

	age	urineDark	sex	urineNeg	SGOT	hemoglobin	urineAlb	total	physical
1	-1.00	-0.00	0.01	0.01	-0.00	-0.00	0.00	-0.00	-0.00
2	0.01	-0.15	0.56	0.53	-0.28	-0.30	0.30	-0.16	0.09
3	-0.00	-0.96	-0.03	-0.11	0.16	0.07	0.02	0.04	0.07

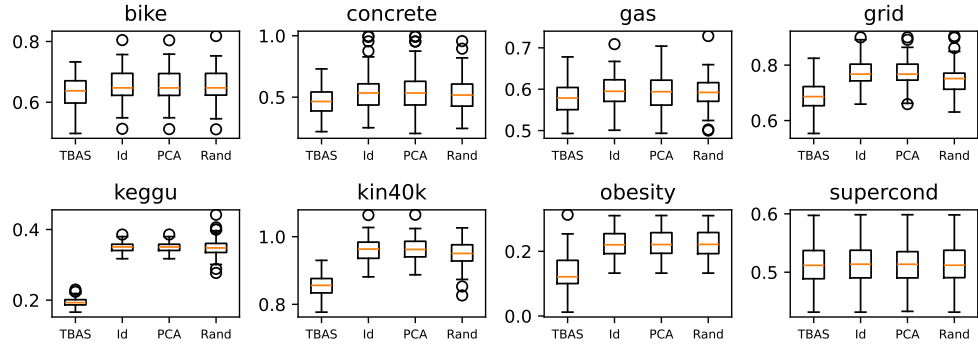
When producing the right panel of Figure 4, we used the prediction after accounting for the effect of age in order to demonstrate the change in the predictive surface over the second and third eigenvalues.

C Numerical Experiments on Classification Trees

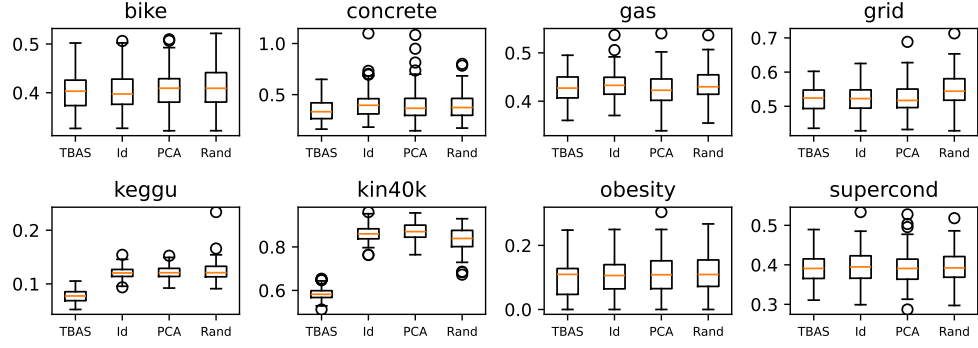
We repeat the experiments of Section 5.1, but now by replacing each regression problem with a classification problem by assessing whether a given observation falls above or below the median observation. The results are given in Figure 7. Intriguingly, the results are significantly less promising

²<https://psdr.readthedocs.io/en/latest/>

Tree Depth 4



Tree Depth 8



Random Forest Depth 4

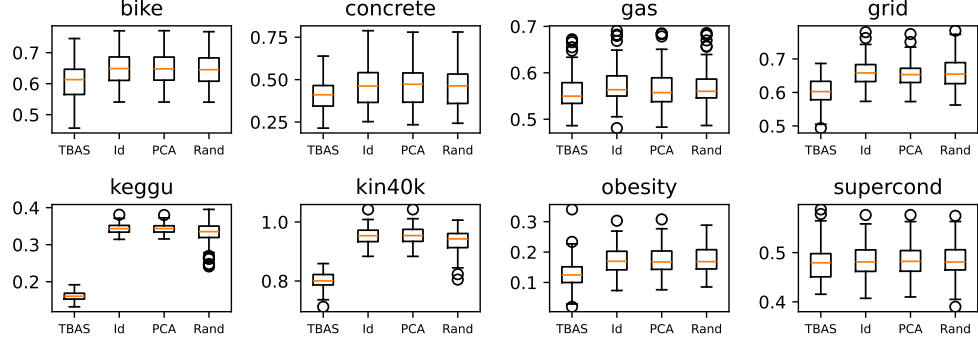


Figure 7: Classification Exercise: Brier Scores are indicated; lower is better.

for the TBAS method, despite the fact that by construction, there is structure in the data that TBAS could possibly exploit. This indicates that there may be special considerations to be taken in deploying this methodology to classification problems.